Learning and Nonlinear Models - Revista da Sociedade Brasileira de Redes Neurais (SBRN), Vol. 3, No. 2, pp. 61-70, 2005

APPROXIMATION METHODS OF OPTICAL SPECTRA: AN ANALYSIS OF THE APPLICATION OF CONSTRUCTIVE RBF NETWORKS IN FIBER OPTIC SENSING

A. S. Paterno[1]
L. V. R. Arruda
H. J. Kalinowski
Universidade Tecnológica Federal do Paraná
80230-901 Curitiba Brazil
Email: [1]sade@cpgei.cefetpr.br

Abstract - This paper reports an analysis of the methods used to interrogate fiber Bragg grating sensors that use the whole reflection spectrum of the sensor. Standard methods like the identification of the peak of the spectrum in the Gaussian or polynomial fit, as well as the direct peak detection in the non-processed data and the determination of the peak by calculation of the centroid of the spectrum are also analyzed. A method recently proposed that uses a constructive Radial-basis function network is analyzed and compared to the other methods, demonstrating that this method produces the lowest uncertainty in the peak determination. A new methodology to find the optimum radius of the radial-basis function for fiber Bragg grating sensor interrogation is proposed. An analysis with respect to characteristics of the acquired data and processing time is also described.
Index terms - Radial-basis function networks, fiber Bragg grating sensors, fiber optic sensors, fiber Bragg grating interrogation.

1. Introduction

Fiber optic Bragg gratings (FBG) have several applications in the fiber-optic field, as for example reflection filters in fiber optic communication systems, being also used to compensate dispersion or working as components of more complex devices such as fiber lasers or amplifiers [1]. They can also work as temperature and mechanical strain sensors, since the profile of the spectrum of the light reflected by them is perturbed by temperature and mechanical strain[2]. The most elementary way to interrogate such sensors consists in acquiring the whole spectrum of the light reflected by the FBG using an optical spectrum analyzer and observing the peak of its spectrum. Since the behavior of the peak will indicate the degree of the perturbation, be it temperature or strain, the analysis of the data acquired by the interrogation system must provide an accurate analysis of the spectrum profile, regardless of noise or some spurious distortion in the signal not related to the analyzed perturbation. When using such an interrogation technique that acquires the whole spectrum of the light reflected by the FBG, one usually fits the spectrum using Gaussian, Lorentzian or polynomial fits, which would cause the peak of the approximated spectrum to be more accurate [3]. The approximation is justified by the fact that a certain level of noise is inevitably present in the acquired experimental spectrum. Recently a method using a constructive radial-basis function (RBF) network in a simpler method than shown in this paper has been proposed reporting satisfactory results [4,5]. The use of a RBF network to approximate FBG spectra can be considered as an extension of the idea of fitting the spectrum profile with a single Gaussian function, if the RBF used in the network is also a Gaussian function. Besides, a performance analysis of the different fitting methods in terms of peak accuracy for the FBG interrogation under different signal-to-noise ratios still remains incomplete. In this paper an analysis of the performance of the newest and most used methods to approximate the FBG sensor spectra is developed using noisy simulated spectra. The evaluated methods are the peak identification of a Gaussian fit under different levels of noise, the peak identification of a polynomial fit when the polynomial function has different orders; the analysis of the position of the peak calculated via the determination of the centroid of the spectrum, and the peak identification in an approximated spectrum using a RBF neural network. The simulations are performed using spectra with different levels of noise and the lowest uncertainty over other methods in the peak identification in the spectra approximated with RBF neural network is demonstrated.

Since the approximation with neural networks can become time-consuming, an analysis of the algorithm shows the behavior of the uncertainty in the approximated peak for different resolutions and consequently different number of points used in the approximation. Consequently, the number of neurons used in the network is determined in a way that it can be feasible to use the algorithm in a practical case, as an add-on software in an optical spectrum analyzer, for example. In order to optimize performance and determine an optimum dimension for the neural network approximation, an algorithm of forward selection [6] using a least-square orthogonalization process [7] is used.

2. Interrogating fiber Bragg grating sensors

A fiber Bragg grating is made by the modulation of the refractive index in the core of a fiber optic [8]. A fiber optic scheme showing the representation of the modulated refractive index in its core is shown in fig. 1, where the profile of the modulation is also presented. This modulation can be imprinted in the fiber optic by exposing its photosensitive core to an interference pattern of ultraviolet light.

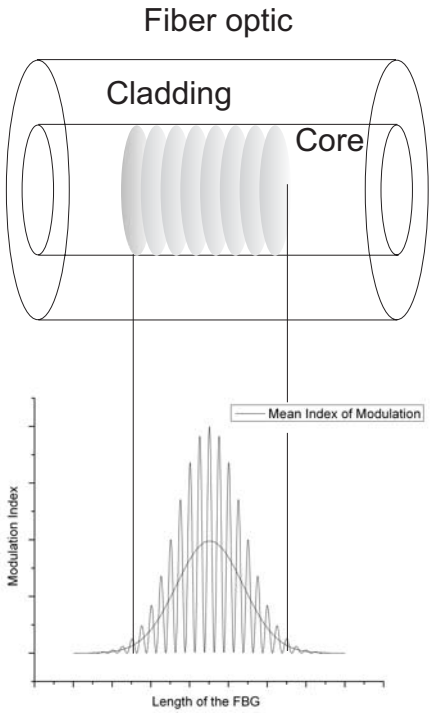

Figure 1- A schematic representation of a FBG showing its index modulation in the core with a gaussian profile.

Therefore, the FBG works as a reflection filter with its band centered at the Bragg wavelength, λ_B, which is a parameter that depends on the period of this modulation, Λ, and on the effective index of refraction of the fundamental mode of the single-mode fiber, n_{eff}. This dependence is expressed by the Bragg condition:

$$\lambda_B = 2n_{eff}\Lambda \tag{1}$$

If the FBG is subject to a uniform field of perturbations, for example, being stretched or heated, the device can work as a point sensor. The effective index of refraction as well as the period of the grating change with temperature and mechanical perturbations. As a consequence, the Bragg wavelength and the center wavelength of the reflected band vary with these perturbations. Strain and temperature variations, $\Delta\varepsilon$ and ΔT, will cause the Bragg wavelength to shift according to:

$$\Delta\lambda_B = \lambda_B(1+p_e)\Delta\varepsilon + \lambda_B(\alpha_n+\alpha_\Lambda)\Delta T \tag{2}$$

where p_e is an effective strain-optic constant. A typical value for the strain sensitivity is about $1.2\,\text{pm}/\mu\text{strain}$ at the wavelength $1550\,\text{nm}$ [1]. The second term in the right side of equation (2) corresponds to the wavelength shift for a temperature variation ΔT, where α_n is the thermo-optic coefficient and α_Λ the thermal expansion coefficient for the fiber optic, giving a typical thermal sensitivity of $10\,\text{pm}/^{\circ}\text{C}$ at $1550\,\text{nm}$ [1].

It is then natural to think of using this device as an intrinsic wavelength encoded temperature and strain sensor. The function of the interrogation system will then be to detect in a wavelength range as accurately as possible the position of the Bragg wavelength, or equivalently the center wavelength of the spectrum, or the centroid of the spectrum.

Although there are several different methods to identify the behavior of the center wavelength of the FBG [8], in this paper, only interrogation methods that use the acquisition of the reflection spectrum of the FBG are analyzed. The acquired data is processed by using a least-squares Gaussian fit, polynomial fits, calculating the centroid of the spectrum and approximating it using the radial-basis function network. This last method is analyzed and described in detail in the following sections.

3. Neural Networks in FBG interrogation

A few techniques using artificial neural networks (ANN) to analyze the acquired reflection spectra from FBG sensors have already been proposed in the literature. The training phase of these ANN consists in exposing the neural network to a series of

previously known reflection spectra [9] or other optical signal that can be associated to the Bragg wavelength, as for example, the signal obtained from a Fabry-Perot interferometer [10]. After the training phase, when exposed to the perturbed spectrum, the ANN can classify the spectrum, obtaining its peak position or other parameter related to the measurand. If the FBG is not a point sensor, other forms of distortions in the spectrum can be classified. These distortions can be produced by a chirp on the FBG caused by debonding of the sensor or even noise in the photodetector. This approach uses the ANN as a pattern classifier.

The use of an ANN to approximate and identify the Bragg wavelength accurately is the extension of an idea that is a common practice when analyzing FBG sensor spectra, namely, the curve fit using usually a Gaussian function. A least-squares curve fit that results in the coefficients (weights) of a series of Gaussian functions to approximate the FBG spectra can be obtained using a special type of ANN: the radial-basis function network. This approximation can be viewed as a fitting problem in a high-dimensional space. For this purpose, a three-layer non-linear radial-Basis function network is proposed to approximate spectra from FBG sensors.

3.1. ANN description

The three-layer architecture of the Radial-basis function network has an input layer with one neuron connected to all neurons in the hidden layer. It receives a vector containing the wavelength points. The input data are made of two elements, the wavelength λ_j and the intensity of the spectrum at this wavelength, $\hat{y}_j$, where j corresponds to the $j-$th point. They are represented by a P-dimensional wavelength vector $\vec{\lambda} = [\lambda_1, \lambda_2, ..., \lambda_P]^t$ and its corresponding spectrum vector $\hat{\mathbf{y}} = [\hat{y}_1, \hat{y}_2, ..., \hat{y}_P]^t$ that is used as a target during the training phase.

The hidden non-linear layer has a Gaussian form and a variable number of neurons, N, such that it has a constructive training phase. Each neuron has an output expressed by:

$$\phi(\lambda, t_i) = \exp\left(-\frac{|\lambda - t_i|^2}{2\sigma^2}\right) \tag{3}$$

where λ is the wavelength, t_i is the position in the spectrum of the i-th RBF, and σ its width. Every RBF has its center coinciding with some element of the vector $\vec{\lambda}$. The width σ is a parameter that is determined experimentally. It is one of the parameters that determines the smoothness of the curve fit and is set to a value that minimizes the peak identification uncertainty. The output layer has one neuron connected to all neurons in the hidden layer and has as output a weighted summation of the hidden layer output, expressed by:

$$F(\lambda) = \omega_1\phi(\lambda, t_1) + \omega_2\phi(\lambda, t_2) + ... + \omega_N\phi(\lambda, t_N) \tag{4}$$

where $\omega_i (i = 1..N)$ are the weights of the synapses connecting the hidden neurons to the output unit.

3.2. RBF network algorithm with forward selection and orthogonalization

In order to find a subset of RBF to approximate the data using equation (4), the algorithm starts with an empty subset, adding one RBF at each step when the error of the approximation is calculated [11]. Every RBF in the wavelength interval is analyzed in a way that it be chosen or rejected to form the approximation function expressed by equation (4).

A model selection criterion called generalized cross-validation (GCV) is used to find out when the process of building the subset of RBF has to stop [11,6]. It is used to estimate the prediction error and the behavior of the model on unknown inputs. The GCV is useful as any other model selection criteria because it can have a minimum near the minimum squared-error. Since one usually does not know the behavior of the error, the GCV value can be used to decide when the model is acceptable. This GCV value decreases when the network is being trained and stops decreasing when it is overtrained. A regularization parameter, γ, is also used, and can be maintained fixed or calculated recursively at each addition of RBF to the design matrix. The use of a model selection criterion value to decide when the training phase ends and the use of a regularization parameter form the basis of the algorithm proposed by Orr in [6]. Here a fixed regularization parameter is used and the algorithm is implemented using MATLAB.

In eq. 5, the expression for the GCV value is shown, where the scalars can be recursively calculated [6]:

$$\mathrm{GCV}_m = \frac{P\left\|\mathbf{P}_m\hat{\mathbf{y}}\right\|^2}{\left[\mathrm{trace}(\mathbf{P}_m)\right]^2} \tag{5}$$

where $\mathbf{P}_m$ is a projection matrix defined in the following eq. 8. A few matrices are useful in the algorithm. The first one is the design matrix that is built by the RBF chosen to be part of the approximation function:

$$\mathbf{H}_m = \begin{bmatrix} \phi(\lambda_1,t_1) & \phi(\lambda_1,t_2) & \dots & \phi(\lambda_1,t_m) \\ \phi(\lambda_2,t_1) & \phi(\lambda_2,t_2) & \dots & \phi(\lambda_2,t_m) \\ \vdots & \vdots & \ddots & \vdots \\ \phi(\lambda_P,t_1) & \phi(\lambda_P,t_2) & \dots & \phi(\lambda_P,t_m) \end{bmatrix} \tag{6}$$

where m represents the variable size of the design matrix, which will depend on the number of RBF used in the approximation and at the end of the training phase $m = N$. The full matrix $\mathbf{F}$ is defined as:

$$\mathbf{F} = [\mathbf{f}_1\mathbf{f}_2\dots\mathbf{f}_P] = \begin{bmatrix} \phi(\lambda_1,\lambda_1) & \phi(\lambda_1,\lambda_2) & \dots & \phi(\lambda_1,\lambda_P) \\ \phi(\lambda_2,\lambda_1) & \phi(\lambda_2,\lambda_2) & \dots & \phi(\lambda_2,\lambda_P) \\ \vdots & \vdots & \ddots & \vdots \\ \phi(\lambda_P,\lambda_1) & \phi(\lambda_P,\lambda_2) & \dots & \phi(\lambda_P,\lambda_P) \end{bmatrix} \tag{7}$$

where $\mathbf{f}_i$ are the columns of whole set of candidate functions to become a RBF in the expansion. The projection matrix is also a useful definition used in the algorithm:

$$\mathbf{P}_m = \mathbf{I}_P - \mathbf{H}_m(\mathbf{H}_m^t\mathbf{H}_m + \gamma\mathbf{I}_m)^{-1}\mathbf{H}_m^t \tag{8}$$

where $\mathbf{I}_m$ is the identity matrix of order *m*. The algorithm then starts by factoring the design matrix into:

$$\mathbf{H}_m = \tilde{\mathbf{H}}_m\mathbf{U}_m \tag{9}$$

where $\tilde{\mathbf{H}}_m$ has $\{\tilde{\mathbf{h}}_i\}_1^m$ as orthogonal columns. $\mathbf{U}_m$ is upper triangular and can be calculated recursively. The approximation problem is then in the form given by:

$$\hat{\mathbf{y}} = \mathbf{H}_m\mathbf{w}_m + \mathbf{e}_m = \tilde{\mathbf{H}}_m\tilde{\mathbf{w}}_m + \mathbf{e}_m \tag{10}$$

where $\mathbf{w}_m$ is the vector with m ordinary weights, $\tilde{\mathbf{w}}_m$ contains the weights associated to the orthogonal design matrix and $\mathbf{e}_m$ has unknown errors between the measured and the true values. The next step consists in adding an orthogonal column from the full matrix $\mathbf{F}$ to the orthogonal design matrix $\tilde{\mathbf{H}}_m$:

$$\tilde{\mathbf{H}}_m = [\tilde{\mathbf{H}}_{m-1}\tilde{\mathbf{f}}_i] \tag{11}$$

where $\tilde{\mathbf{f}}_i$ can be calculated from:

$$\tilde{\mathbf{f}}_i = \mathbf{f}_i - \sum_{j=1}^{m-1}\frac{\mathbf{f}_i^t\tilde{\mathbf{h}}_j}{\tilde{\mathbf{h}}_j^t\tilde{\mathbf{h}}_j}\tilde{\mathbf{h}}_j \tag{12}$$

The operation in equation (12) makes the added column orthogonal to the design matrix. The cost function to be

minimized has a matrix representation given by $\tilde{E}_m^{(i)} = \hat{\mathbf{y}}^t \mathbf{P}_m \hat{\mathbf{y}}$ and matrix $\mathbf{P}_m$ is calculated using equation (8). If $\mathbf{f}_i$ minimizes the cost function or maximizes:

$$\tilde{E}_{m-1} - \tilde{E}_m^{(i)} = \frac{(\hat{\mathbf{y}}^t \tilde{\mathbf{f}}_i)^2}{\gamma + \tilde{\mathbf{f}}_i^t \tilde{\mathbf{f}}_i} \tag{13}$$

then it becomes a column of the design matrix ($\tilde{\mathbf{h}}_m = \tilde{\mathbf{f}}_i$). The operation of equation (13) has to be performed for every column which is a candidate to become a RBF. To calculate $\mathbf{w}_m$, it is necessary to determine $\tilde{\mathbf{w}}_m$, where its j-th component is:

$$(\tilde{\mathbf{w}}_m)_j = \frac{\hat{\mathbf{y}}^t \tilde{\mathbf{h}}_j}{\gamma + \tilde{\mathbf{h}}_j^t \tilde{\mathbf{h}}_j}, \quad 1 \le j \le m \tag{14}$$

It is then possible to obtain $\mathbf{w}_m$ using $\mathbf{U}_m$ and $\tilde{\mathbf{w}}_m = \mathbf{U}_m \mathbf{w}_m$. The upper triangular matrix $\mathbf{U}_m$ is calculated recursively by:

$$\mathbf{U}_m = \begin{bmatrix} \mathbf{U}_{m-1} & (\tilde{\mathbf{H}}_{m-1}^t \tilde{\mathbf{H}}_{m-1})^{-1} \tilde{\mathbf{H}}_{m-1}^t \mathbf{f}_i \\ \mathbf{0}^t{}_{m-1} & 1 \end{bmatrix} \tag{15}$$

setting $\mathbf{U}_1 = 1$. The training and performance of the RBF network and the optimization of its parameters are discussed in the section following the performance analysis of the methods to which the network is compared.

4. Methodology of the analysis

The reflection spectrum of a simulated FBG will have its peak identified in the approximation using least-squares polynomial fits of several orders, a least-squares Gaussian fit and the approximation with the RBF network. A direct peak measurement in the raw data spectrum is also obtained and the centroid of these spectra is calculated. The peak of the approximated spectrum is obtained by determining the maximum intensity position in the approximated data. The peak wavelength, λ_B, is considered a random variable and its standard deviation, σ_u, is considered the uncertainty of the method for a given signal-to-noise ratio in the raw data. This value is a measure of how accurate the method of identifying the peak can be. This uncertainty can be translated into the units of the measurand. If one considers the sensitivities of a FBG sensor as stated in section 2, an error of $40\,\mu$strain in a sensor system measuring strain, or $4\,^{\circ}$C measuring temperature, would correspond to approximately 40 pm in wavelength. Such values for the error are usually a tolerable margin for an industrial sensor system.

There are basically two types of FBG spectra used in fiber sensing: the uniform and apodized spectra. The uniform FBG profile has a uniform refractive index modulation along the whole sensor and this modulation starts and terminates abruptly at the begin and end of the device. This type of FBG produces a uniform spectrum. This spectrum has several side-lobes as shown in fig. 2(left). This is an effect similar to the one that happens when using digital filters with truncated data. The spectral response of such filters has several side-lobes.

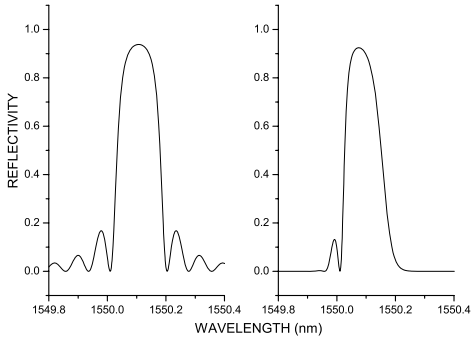

Figure 2 - Spectrum of the light reflected by a uniform FBG. Side-lobes are caused by the abrupt termination of the modulation in the index of refraction in a uniform FBG (left). Side-lobes are almost completely supressed in the spectrum of an apodized FBG (right).

In order to minimize such effect, windowing is applied [12]. This windowing in FBG fabrication corresponds to a technique called apodization [13] in which the profile of the index modulation is smoothed along the FBG, having usually a gaussian function as an envelope of this modulation. The resulting spectra of apodized FBG have the side-lobes minimized, as shown in fig. 2 (right).

Methodology to calculate the standard deviation of the peak: uncertainty determination

The FBG spectra are simulated using a transfer-matrix technique [14] and pseudo-random noise is added to each approximated spectrum. A series of 50 spectra is calculated and for a given noise level, the peaks of the 50 spectra are determined and the standard deviation of the set of peaks is calculated. This standard deviation value for a given SNR is the uncertainty of the peak identification method. A wavelength sample space of 1 pm is used in all simulations, unless otherwise specified. An illustration of the spectra obtained through the approximation using the RBF network, an experimental spectrum with 25 dB SNR and a Gaussian fit are depicted in fig. 3 together with the values found for each spectrum.

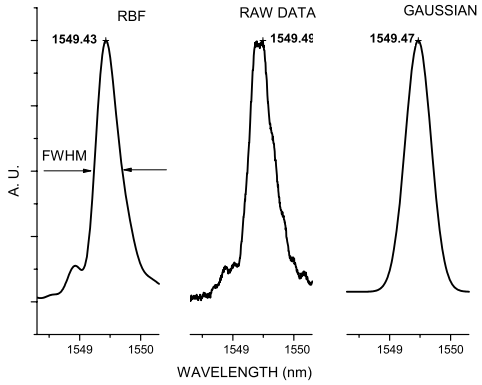

Figure 3 - Raw data spectrum and its approximations: RBF approximation (left), raw data spectrum (middle) and Gaussian fit (right). In the RBF approximation, the Full-Width at Half Maximum (FWHM) in the spectrum is indicated.

4.1. Direct peak identification and centroid calculation

The determination of the peak of a spectrum by finding the wavelength position at which the intensity is maximum causes the highest uncertainty, since the spectrum is not subject to any kind of processing or filtering. The centroid calculation to determine the peak is based on the geometrical determination of the spectrum centroid, in a way that it is dependent on the set of points used to calculate λ_C [8], as expressed by:

$$\lambda_C = \frac{\sum_{j=1}^{N} \lambda_j \hat{y}_j}{\sum_{j=1}^{N} \hat{y}_j} \tag{16}$$

where λ_C represents the centroid wavelength of the spectrum and $|\lambda_1 - \lambda_N|$ is the width of the interval for the calculation of the parameter. This method has a higher uncertainty if the peak of the spectrum is not located at the center of the data set used

in the centroid calculation. Moreover, if the used spectrum is apodized, the uncertainty is still higher, because the data will not have a peak exactly at the center point of the spectrum. In this case, choosing the correct set of data to find the peak is the most critical task. A picture depicting the uncertainty for the direct peak identification and the centroid calculation is shown in fig. 4.

4.2. Peak identification in polynomial approximation

In order to provide the uncertainty behavior of the peak identification using least-squares polynomial approximations, it is demonstrated that an increase in the order of the polynomial used in the fit adds a positive offset to the uncertainty curve of the peak identification. The uncertainty curves are plotted and depicted in fig. 4 for polynomial approximations with orders varying from 2 to 4. It is observed that a second-order polynomial fit shows the lowest uncertainty and polynomials with orders higher than 4 show a non-zero uncertainty even under very low noise in the spectrum, that is, with signal-to-noise ratios higher than 30 dB. It is important to notice that this data were obtained using only a segment of the spectrum determined by the wavelength interval containing the intensities values up to 30% smaller than the peak intensity.

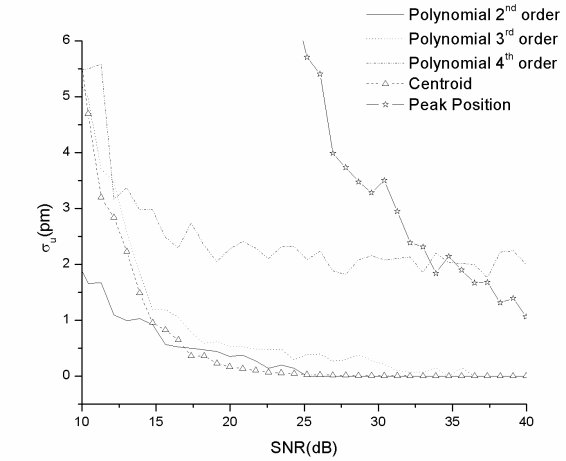

Figure 4 - Uncertainty curves for the peak identification in spectra approximated with polynomial fits of orders 2, 3 and 4, for the method using the centroid calculation and the method using peak position in the raw spectrum.

4.3. Gaussian approximations

Compared to the previously cited methods, the Gaussian approximation provides the second lowest uncertainty for SNR values higher than 20 dB. The centroid method sets a lower limit for this interval, as shown in fig. 5. However, the drawback of the least-squares Gaussian fit resides in the fact that it usually needs an estimate of the peak position in the curve to be approximated. The point corresponding to the peak position can be refined during a recursive approximation process. As a consequence, the peak that is to be obtained must be initially guessed, even if it is unknown. In fig. 5, the uncertainty curves for the comparison of the previous methods are shown, demonstrating that the centroid method establishes a floor for the previously cited methods for SNR higher than 20 dB. All the methods provide comparable uncertainty results, with the exception of the direct peak detection.

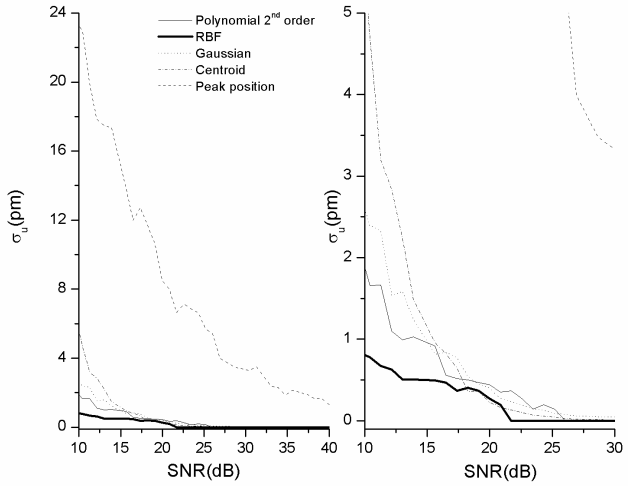

Figure 5. - Uncertainty curves for the peak identification in spectra using direct peak identification, the centroid method, second-order polynomial fit, Gaussian fit and peak determination in the RBF approximation. On the right side, the same graph is plotted with the uncertainty axis rescaled such as to allow a better comparison of the curves.

4.4. RBF approximation: training and optimizing network parameters

As discussed in section 2, the algorithm is characterized by a set of parameters that determine the smoothness with which it is going to approximate the spectra. Some of these parameters can be estimated automatically or set fixed during the training phase. The regularization parameter, γ, can be calculated automatically or set fixed to a value about 10^{-9} in the studied case. This value is estimated by deriving the generalized cross-validation (GCV) parameter and finding a recursive formula to estimate it each time a RBF is added to the base [6]. Depending on its value the approximation is smoother or tighter.

The degree of smoothness is also related to the width of the RBF, σ. Setting a value for the radius is a more flexible way to determine how tight the approximation can be without worrying about convergence problems. Convergence may be a problem when the regularization parameter is calculated recursively [6]. There is no direct analytic formula to determine the radius of the RBF function that provides an optimal approximation [15]. Therefore, it is not direct to establish in the spectrum case a quantitative parameter to define the smoothness degree as a function of the RBF radius. It is then here proposed an evaluation of the radius that determines a minimal uncertainty curve. The radius of the RBF is then set experimentally to a value that minimizes the uncertainty in the peak identification. To illustrate this behavior, different uncertainty curves are plotted in fig. 6 as a function of the signal-to-noise ratio, and for different radius of the RBF in the approximation. The reference radius is the bandwidth of the FBG spectrum, defined by the full-width at half maximum (FWHM) illustrated in the RBF approximation in fig. 3.

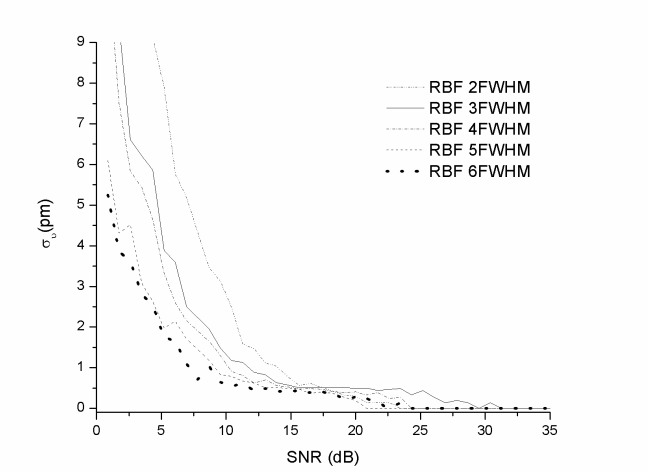

Figure 6 - Uncertainty curves for the RBF approximation. Each curve corresponds to an approximation in which the RBF radius is 2FWHM, 3FWHM, 4FWHM, 5FWHM and 6FWHM.

The choice of a radius is not absolutely free. If the radius is too large, the approximation may lose its capacity to approximate specific characteristics of the curve. In this case, the dimension of the approximation is lower. If the radius is too small, the approximation may be too tight and the noise present in the processed data is also approximated. In this case, the dimension N of the RBF network is higher and the processing time also increases. In fig. 3, the RBF approximation used a radius σ=FWHM, which resulted in a dimension of N=25 RBF in the expansion.

The lowest uncertainty is obtained with a radius around σ=6FWHM. If the radius is larger, the uncertainty is also increased. As can be observed in fig. 5, the uncertainty curve for the RBF approximation using a radius σ=6FWHM is plotted together with the curves for the other methods. For this radius, the uncertainty is the lowest amongst all of the analyzed methods, setting a lower limit for the uncertainty in peak identification. In this case, the dimension of the approximation can reach N=5 depending also on the width of the processed wavelength interval.

4.5. Sample space resolution and spectrum profile

It must be observed that the previous optimized parameters are obtained for a given spectrum profile characterized by a reflectivity of 93.9% and a 1pm wavelength sample space. When choosing the FBG sensor working as a point sensor, one has to consider that the spectrum must not be flat around the peak. The flatness of the region around the peak of the spectrum is a direct function of the index of modulation in the refractive index structure that forms the FBG. For strong FBG, that is, with a relatively high index of modulation, the spectrum tends to saturate and have a flat top that may increase the uncertainty in experimental measurements [1,8,13]. Such strong FBG are not usual as FBG sensors. A reflectivity of 93.9% is simulated such as to be representative of a typical FBG sensor with a non-flat region around the peak. To illustrate the behaviour of the uncertainty for the RBF network and wavelength sample spaces of 1pm and 5pm, the graphs in fig. 7 are depicted. It is observed in this figure that an increase in the wavelength sample space causes the uncertainty to increase. The uncertainty curves for a weak FBG with a spectrum with 46.5% maximum reflectivity and different wavelength sample space are also shown.

The FBG spectrum with 46.5% maximum reflectivity has a less flat region around the peak. The methodology described in the previous section is used to find the radius in the RBF network that provides the lowest uncertainty, σ=3FWHM. A change to a lower reflectivity, although it changes the signal-to-noise ratio, does not alter significantly the uncertainty curve as can be seen in fig. 7. The larger wavelength sample space causes the uncertainty curve to have an oscillatory behavior, due to the larger step in the quantization of the spectrum data. The higher wavelength sample space causes the uncertainty to increase for both values of reflectivity.

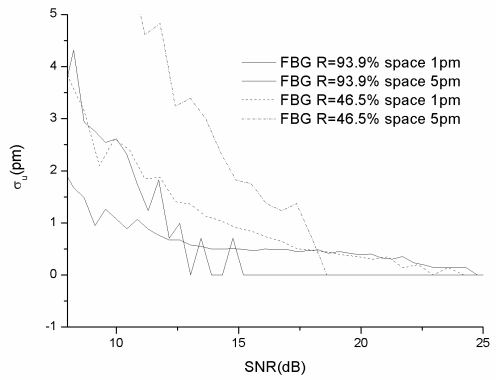

Figure 7 - Uncertainty curves for the RBF approximation processed with different wavelength sample spaces of 1 pm and 5 pm and peak reflectivity of 46.5% and 93.9%.

5. RBF network complexity and processing time

The approximation happens every time the network receives a new spectrum. Consequently, training and generalization makes up the process of approximation and makes the algorithm heavily dependent on the number of points used in the acquired spectrum. Besides, the algorithm is a set of repeatedly executed matrix operations and it is natural to think of implementing the algorithm in a processor with a parallel architecture or in a neurocomputing chip. In a personal computer with the algorithm implemented with MATLAB, the drawback of using a high number of points per spectrum becomes evident and that is the reason why an algorithm of forward selection with an orthogonalization process is used. The forward selection with the proper choice of the RBF radius and regularization parameter minimizes the number of RBF used in the expansion. The orthogonalization process makes the number of floating point operations proportional to the number of processed points, *P*. This is the number of operations performed to add one RBF to the design matrix. Without orthogonalization this number would be proportional to P^2. If even with these techniques the algorithm is still time-consuming, a policy to choose a section of the processed spectrum containing the peak has to be implemented. With such a window, the number of possible RBF candidates, N, to be added to the design matrix is reduced and the processing time for the expansion is proportional, to first order, to $P \times N$ [6]. Roughly comparing, a standard least-squares regression in a Gaussian fit and the RBF network require the same time to process a spectrum with P=300 points using a standard personal computer and the MATLAB algorithm.

6. Conclusion

An analysis of the newest and most used methods in FBG interrogation is demonstrated. The analysis with respect to Gaussian and polynomial fit, and to centroid calculation and direct peak detection is reported showing similar results to the results obtained in the literature [3]. An analysis of the recently proposed method that uses a RBF network to approximate the spectrum shows a better performance in terms of uncertainty if compared to the other presented methods. A methodology to find out the best radius of the RBF network is proposed by choosing the value of the radius that produces the lowest uncertainty in the peak determination. In this case the peak of the spectrum that is associated to the measurand of the sensor is considered a random variable. This methodology also allows the user to implement an algorithm that can have the time performance that a Gaussian fit produces, if the correct resolution and number of points in the acquired spectrum are used. If this correct policy is implemented, the algorithm can be used to interrogate sensors with dynamic behavior, since in this case the time performance is no longer a problem.

7. Acknowledgments

The authors would like to thank the Agência Nacional do Petróleo (ANP) and the Financiadora de Estudos e Projetos (FINEP) for the financial support by means of the Human Resources Program of the ANP in the Gas and Oil Sector (PRH-ANP/MCT - PRH10 - UTFPR). CNPq, CAPES and Fundação Araucária (Brazilian agencies) are also aknowledged.

References

[1] K. O. Hill and G. Meltz: “Fiber Bragg grating technology fundamentals and overview”, Journal of Lightwave Technology, vol. 15, no. 8, pp. 1263–1276, 1997.
[2] A. D. Kersey, M. A. Davis, H. J. Patrick, M. LeBlanc, K. P. Koo, C. G. Askins, M. A. Putnam, and E. J. Friebele: “Fiber

grating sensors", Journal of Lightwave Technology, vol. 15, no. 8, pp. 1442–1463, 1997.
[3] S. D. Dyer, P. A. Williams, J. D. Kofler, R. J. Espejo, and S. M. Etzel: "Fundamental limits in fiber Bragg grating peak wavelength measurements", 17th International Conference on Optical Fibre Sensors - Proceedings of the SPIE, vol. 5622, pp. 88–93, 2005.
[4] A. S. Paterno, L. V. Arruda, and H. J. Kalinowski: "Radial-basis function network for the approximation of quasi-distributed FBG sensor spectra with distorted peaks", 17th International Conference on Optical Fibre Sensors - Proceedings of the SPIE, vol. 5622, pp. 976–980, 2005.
[5] A. S. Paterno, J. C. C. Silva, M. S. Milczewski, L. V. R. Arruda, and H. J. Kalinowski: "Radial-basis function network for the approximation of FBG sensor spectra with distorted peaks", Measurement Science and Technology, vol. 17, pp. 1039-1045, 2006.
[6] M. J. L. Orr, "Regularisation in the selection of radial basis function centres", Neural Computation, vol. 7, pp. 606–623, 1995.
[7] S. Chen, C. F. N. Cowan, and P. M. Grant: "Orthogonal least squares learning algorithm for radial basis function networks", IEEE Transactions on Neural Networks, vol. 2, pp. 302–308, 1991.
[8] A. Othonos and K. Kalli, Fiber Bragg Gratings: Fundamentals and Applications in Telecommunications and Sensing. Boston - Artech House, 1999.
[9] C. C. Chan, C. Z. Shi, W. Jin, and D. N. Wang: "Improving the wavelength detection accuracy of FBG sensors using an adaline network", IEEE Photonics Technology Letters, vol. 15, pp. 1126–1128, 2003.
[10] R. de Oliveira, O. Frazão, J. L. Santos, and A. T. Marques: "Optic fibre sensor for real-time damage detection in smart composite", Computers and Structures, vol. 82, pp. 1315–1321, 2003.
[11] S. Haykin, *Neural Networks*. New Jersey: Prentice-Hall, 1999.
[12] A. V. Oppenheim and R. W. Schafer, Discrete-Time Signal Processing. New Jersey: Prentice-Hall, 1989.
[13] R. Kashyap: *Fiber Bragg Gratings*. London: Academic Press, 1999.
[14] M. Yamada and K. Sakuda: "Analysis of almost-periodic distributed feedback slab waveguides via a fundamental matrix approach", Applied Optics, vol. 26, no. 16, p. 3474–3478, 1987.
[15] M. Orr: "Optimising the widths of radial-basis functions", Fifth Brazilian Symposium on Neural Networks - Belo Horizonte - Brazil, 1998.